Modelling the Pressure Profile for Optical Cables in Ducts

Almar Snippe[1,2], Onno R. Bresser[3], Sipke Hoekstra[1], Willem Griffioen[4]

[1]University of Twente, De Horst 2, 7522 LW Enschede, Netherlands

[2] BV Twentsche Kabelfabriek, Spinnerstraat 15, 7481 KJ Haaksbergen, Netherlands

[3] TKH Group NV, Spinnerstraat 15, 7481 KJ Haaksbergen, Netherlands

[4] Plumettaz SA, Wijnhaven 105, 3011 WN Rotterdam, Netherlands

+31-53-4891036 · a.snippe@utwente.nl

Abstract

The longitudinal pressure profile is an important parameter when calculating the correct blowing force during the process of installing optical fiber cables using the viscous flow of air. This paper presents a model of the pressure inside the duct that contains a moving cable. This new model of the pressure profile is used to calculate the blowing force and the force build-up in the cable more accurately. Therefore, the estimation accuracy and reliability of the maximum installation length of optical fibers is increased.

Keywords: Longitudinal pressure profile; cable; duct; jetting; blowing; force build-up; installation length.

1. Introduction

Optical fibers have been installed in ducts by exploiting the viscous flow of air for over twenty years now. It has emerged that the synergy of pushing and blowing a cable simultaneously leads to longer installation lengths than solely pushing or pulling [2]. During this process, the pressure decay along the length of the duct is one of the key parameters that propels the cable. The pressure decay depends on the pressure at the inlet, the atmospheric pressure and the length of the trajectory. This relation is described in the work of Griffioen [2]. However, Griffioen's model is for an empty duct and it is to be expected that the pressure decay will change as a cable moves through the duct. Therefore, this paper presents a model that combines the model of the previously mentioned pressure decay [2] and a model of the pressure at a diameter transition [2]. Based on this new model of the pressure decay, longer installation lengths can be reached which have been experienced in practice.

1.1 Jetting

Jetting is a technique that combines a mechanical pushing force with the viscous flow of air to install optical fibers in pre-installed ducts. In this process a jetting machine is used. This jetting machine is on one side connected to the duct and from the other side the cable is fed through the machine into the duct. Inside the machine, first the cable experiences a mechanical push by either a turning wheel or a caterpillar track. Next, the cable enters an air-tight chamber with a desired pressure. Finally, the cable enters the duct together with the pressurized air. The mechanical push of the turning wheel or the caterpillar track can be generated either hydraulic or pneumatic. The maximum pushing force of the machine stretches from 25 N to 700 N, depending on the machine and the target cable. Obviously, applying a too large force will damage the cable; performing a crash test to determine the maximum pushing force is required for every combination of cable, duct and jet. Furthermore, not every machine is suitable for every cable or tube. Therefore, different combinations of cable and tube require different jetting machines.

2. Theoretical Background

This section presents the theoretical background for jetting cables and the hypothesis that has been formed based on currently used models.

2.1 Griffioen's Model

Griffioen's model [2] calculates the force build-up F in the cable based on the friction force and two propelling forces. The friction force consists of four components, being:

1. Friction due to the dragging of the cable along the duct (linear friction)
2. Friction due to windings in the trajectory
3. Friction due to buckling of the cable
4. Friction due to bends in the trajectory

The two propelling forces are both related to the viscous flow of the air in the duct:

1. Hydrostatic force
2. Hydrodynamic force

2.1.1 Linear Friction

The friction due to dragging of the cable along the duct F_{dr} depends on the friction coefficient f of the two surfaces (cable and duct) and the uniform weight W of the cable in N/m:

$$\mathrm{d}F_{dr}(x) := fW\,\mathrm{d}x. \tag{1}$$

2.1.2 Friction Due to Windings

To calculate the friction due to windings, the normal force per unit of length in windings due to stiffness, W_b, is required [3]:

$$W_b := \frac{384 \cdot A_{eff} \cdot B}{P^4}$$

where B is the stiffness of the cable in Nm^2 and P is the period of the (sine-shaped) windings in m. A_{eff} is the effective amplitude of the windings which is different for a different force build-up. This means that when the cable experiences a pushing force (in Griffioen's model represented by a negative force build-up) the effective amplitude will be different as for a pulling force (a positive force build-up) [3]:

$$A_{eff}(x) := \begin{cases} A + 1/2 \cdot (D_d - D_c), & \text{for } F(x) \geq 0 \\ A - 1/2 \cdot (D_d - D_c), & \text{for } F(x) < 0 \end{cases}$$

where A is the actual amplitude of the windings in m and D_c and D_d are the diameter of the cable and the inner diameter of the duct in m

respectively. Furthermore, the measure $\mathcal{T}$, indicating how tortuous a duct trajectory is, also depends on A_{eff}:

$$\mathcal{T} := \frac{8\pi A_{eff}}{P^2}.$$

The friction due to windings F_w is given by

$$\mathrm{d}F_w(x) := \begin{cases} f(W_b - \mathcal{T}F(x))\,\mathrm{d}x, & \text{for } F(x) \geq 0 \\ f(W_b + \mathcal{T}F(x))\,\mathrm{d}x, & \text{for } F(x) < 0 \end{cases} \tag{2}$$

where F is the force build-up in the cable in N.

2.1.3 Friction Due to Buckling

The friction due to buckling only occurs when the cable experiences pushing forces, i.e. a negative force build-up. In order to calculate the friction due to buckling, the buckling coefficient $\mathcal{B}$ is used:

$$\mathcal{B} := \frac{D_d - D_c}{\pi^2 B}.$$

The friction due to buckling $F_\mathcal{B}$ is given by

$$\mathrm{d}F_\mathcal{B}(x) := \begin{cases} 0\,\mathrm{d}x, & \text{for } F(x) \geq 0 \\ \mathcal{B}F^2(x)\,\mathrm{d}x, & \text{for } F(x) < 0. \end{cases} \tag{3}$$

2.1.4 Friction Due to Bends

The friction due to bends only occurs in bends; in other parts of the trajectory the nett contribution of this friction component to the force build-up is zero. However, the increased force build-up after a bend indirectly affects the force build-up in the rest of the trajectory. The friction in a bend F_b is given by

$$\mathrm{d}F_b = fF\,\mathrm{d}\theta$$

where f is the friction coefficient, F is the force build-up and θ is the angle in radians. This equation will be transformed using the relation between the distance x and the angle θ:

$$\frac{\mathrm{d}\theta}{\mathrm{d}x} = \frac{1}{R}$$

where R is the radius of the bend in m. The friction due to a bend F_b is given by the following equation.

$$\mathrm{d}F_b(x) := \begin{cases} 0\,\mathrm{d}x, & \text{for } x \text{ outside bend} \\ \frac{1}{R}fF(x)\,\mathrm{d}x, & \text{for } x \text{ inside bend} \end{cases} \tag{4}$$

2.1.5 Total Friction Force

Combining Equations 1, 2, 3 and 4 leads to an equation for the total friction force F_f:

$$\mathrm{d}F_f(x) := \left[\sqrt{\mathrm{d}F_{dr}^2(x) + \mathrm{d}F_w^2(x) + \mathrm{d}F_\mathcal{B}^2(x) + \mathrm{d}F_b^2(x)}\right]\mathrm{d}x. \tag{5}$$

Next, the two propelling forces will be discussed.

2.1.6 Pressure Decay

Since both the hydrostatic force and the hydrodynamic force are related to the pressure decay of the air in the duct, the latter is discussed first.

Griffioen's model threats the flow as locally incompressible which allows the use of the following unique relation between the drag coefficient C_d and the pressure decay $\mathrm{d}p/\mathrm{d}x$:

$$\frac{\mathrm{d}p}{\mathrm{d}x} = -\frac{1}{2}C_d \cdot \frac{\rho\bar{v}^2}{D_h} \tag{6}$$

where the drag coefficient is a function of the Reynolds number Re, defined as

$$Re := \frac{\rho\bar{v}D_h}{\mu}. \tag{7}$$

In the above equations ρ is the density of the air in kg/m^3, $\bar{v}$ is the average velocity of the flowing air at a certain point in the duct in m/s, μ is the viscosity of the air in kg/m/s and D_h is the hydraulic diameter in meters. The Reynolds number is dimensionless and it indicates whether a flow is laminar ($Re < 2000$) or turbulent ($Re > 4000$). In the application of blowing cables, the flow is almost always turbulent, i.e. the Reynolds number is large.

Furthermore, when assuming that the velocity of the air is well below the Mach number; the flow is isothermal and the air behaves like an ideal gas, the pressure decay can be described as [2]:

$$\frac{\mathrm{d}p}{\mathrm{d}x} := -\frac{p_1^2 - p_2^2}{2L\sqrt{p_1^2 - (p_1^2 - p_2^2)\frac{x}{L}}} \tag{8}$$

where p_1 and p_2 are the pressure at the inlet and the atmospheric pressure in Pascal respectively and L is the length of the trajectory in meters. The corresponding pressure is given by

$$p(x) := \sqrt{p_1^2 - (p_1^2 - p_2^2)\frac{x}{L}}. \tag{9}$$

where x is the location in the duct in m.

2.1.7 Hydrostatic Force

The hydrostatic force F_{hs}, is a force due to pushing the cable in a pressured space. This force depends on the pressure decay and the cross-sectional area of the cable:

$$\mathrm{d}F_{hs} := -\frac{\pi}{4}D_c^2 \cdot \frac{\mathrm{d}p}{\mathrm{d}x}\,\mathrm{d}x \tag{10}$$

where D_c is the diameter of the cable in meters. Note that a force F_i is always necessary to feed the cable in the pressured duct.

$$F_i := \frac{\pi}{4}D_c^2 \cdot (p_1 - p_2) \tag{11}$$

2.1.8 Hydrodynamic Force

The hydrodynamic force F_{hd}, is a force due to the friction between the cable and the (viscous flow of) air. The hydrodynamic force is highly dependent on the pressure decay as well as on the diameter of the cable and the annulus between the cable and the duct where the air flows:

$$\mathrm{d}F_{hd} := -\frac{\pi}{4}D_c(D_d - D_c)\frac{\mathrm{d}p}{\mathrm{d}x}\,\mathrm{d}x \tag{12}$$

where D_c and D_d are the diameter of the cable and the inner diameter of the duct in m respectively. Note that the pressure decay $\mathrm{d}p/\mathrm{d}x$ is always negative, hence the hydrodynamic force is positive.

2.1.9 Total Blowing Force

Combining Equations 10 and 12 results in an equation for the total blowing force F_{bl} which is the propelling force on the cable due to the airflow:

$$\begin{aligned} \mathrm{d}F_{bl} &:= \mathrm{d}F_{hs} + \mathrm{d}F_{hd} \\ &= -\frac{\pi}{4}D_cD_d\frac{\mathrm{d}p}{\mathrm{d}x}\,\mathrm{d}x \end{aligned} \tag{13}$$

Note that a force F_i (11) is always necessary to feed the cable into the pressured duct.

2.1.10 Force Build-up

The calculation of the force build-up can best be explained by means of an illustration. Figure 1 shows the forces acting on a small slice of cable dx, where F is the force build-up and dF is the force build-up over a small slice of cable dx. The sum of all these

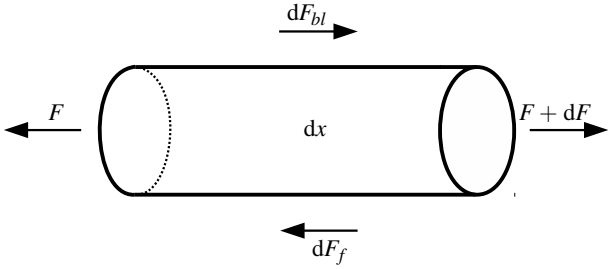

Figure 1: The forces acting on a small slice of cable dx.

forces must be equal to zero due to Newton's first law, hence

$$\begin{aligned} 0 &= F + \mathrm{d}F - F - \mathrm{d}F_f + \mathrm{d}F_{bl} \\ \mathrm{d}F &:= \mathrm{d}F_f - \mathrm{d}F_{bl}. \end{aligned} \tag{14}$$

So, the force build-up F (14) is the difference between the total friction force (5) and the total blowing force (13).
Note that this equation is recursive, i.e. F_w, $F_{\mathcal{B}}$ and F_b (and hence F_f as well) depend on F. Therefore, the force build-up will be calculated numerically, starting at the head of the cable. The force build-up is said to be zero at the head of the cable which is the starting point for the backwards iteration. An example of the force build-up in a cable for a trajectory without bends is shown in Figure 2.

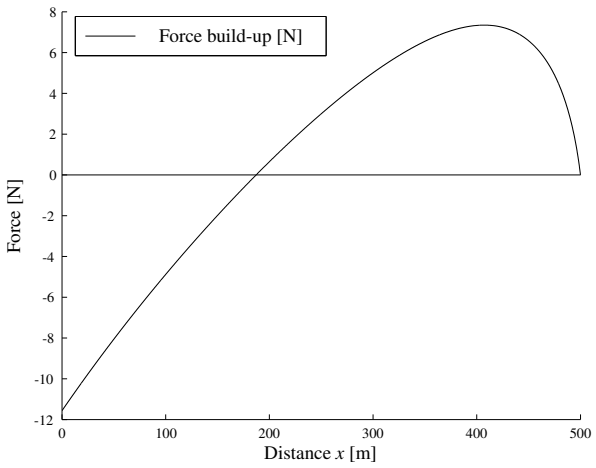

Figure 2: The force build-up for a 7 mm cable in a 10 mm duct of 500 meters and a pressure at the inlet of 10 bar. Negative forces are pushing forces.

2.2 Hypothesis

The hypothesis is that directly after the cable head the air will expand, causing a pressure drop at that point. Therefore, instead of being independent of the cable head position, the pressure will change as the cable advances through the duct. The point of the cable head will be treated as a (moving) diameter transition.
To obtain the pressure at a diameter transition, Griffioen's model [2] uses Blasius' empirical formula for the drag coefficient C_d for a turbulent flow:

$$C_d = \frac{0.31}{Re^{0.25}}$$

However, recently Griffioen presented an approximation that also incorporates the roughness of the ducts used in the installation of optical fibers [1]. This is also the drag coefficient that will be used in this paper:

$$C_d := \frac{0.041}{Re^{0.052}} \tag{15}$$

The pressure p_h at the point X of the cable head is given by the equation for a diameter transition [2]:

$$p_h(X) := \sqrt{\frac{(L-X)p_1^2 D_r^{4.948} + X p_2^2 D_d^{4.948}}{(L-X)D_r^{4.948} + X D_d^{4.948}}} \tag{16}$$

with L being the length of the duct in meters, $X \in [0,L]$, p_1 and p_2 being the pressure at the inlet and the atmospheric pressure respectively, and D_r being the resulting diameter for the part of the duct where the cable is inside:

$$D_r := \sqrt{D_d^2 - D_c^2}.$$

Instead of using just one equation to describe the pressure inside the duct, two equations will be used for every position of the cable head. For every position X of the cable head, the pressure inside the entire duct is given by the pressures p_c and p_e, representing the part of the duct containing the cable and the part without respectively [2]:

$$p_c(x,X) := \sqrt{p_1^2 - (p_1^2 - p_h(X)^2)\frac{x}{X}}$$

with $x \in [0,X]$ and $X \in (0,L]$, and

$$p_e(x,X) := \sqrt{p_h(X)^2 - (p_h(X)^2 - p_2^2)\frac{x-X}{L-X}}$$

with $x \in (X,L]$ and $X \in [0,L)$.
Combining these two equations gives the equation for the pressure p at every point x in the duct for every position X of the cable head:

$$p(x,X) := \begin{cases} p_c(x), \text{ for } x \in [0,X] \text{ and } X \in (0,L] \\ p_e(x), \text{ for } x \in (X,L] \text{ and } X \in [0,L). \end{cases} \tag{17}$$

Figure 3 shows the pressure in the duct according to Equation 17 for an empty duct, it also shows the pressure profile when the cable is pushed halfway through the duct, again applying Equation 17. In these examples, the inner diameter of the duct is 10 mm and the cable has a diameter of 7.8 mm. The pressure at the entrance is 10 bar and the length of the trajectory is 500 meter.
The pressure profile for an empty duct shown in Figure 3 (solid) is the same as that used in the original model [2] regardless of the position of the cable head. So these two examples also illustrate the difference between the original (static) and the new (dynamic) pressure profile.

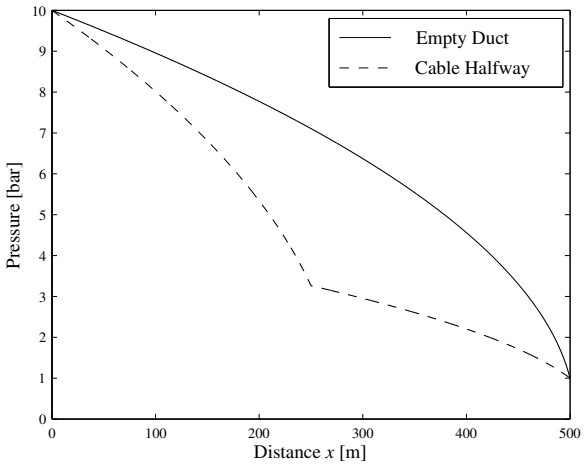

Figure 3: The pressure profile for an empty duct (solid) and for the same duct where the cable is pushed through halfway (dashed). The inner diameter of the duct is 10 mm, the diameter of the cable is 7.8 mm, the length of the trajectory is 500 m, the pressure at the inlet is 10 bar and the atmospheric pressure is 1 bar.

3. Test Set-up and Method

3.1 General Set-up

All tests were performed within the test trajectory in Haaksbergen, the Netherlands. A duct with a length of 500 meters was manipulated in such a way that after every 50 meters a manometer could be attached to measure the pressure at that specific point. The first measurement point was immediately after the installation jet, i.e. the measurement was at 0 meters.

To achieve the required initial pressure, first the cable was pushed into the duct until after the first measurement point (at 0 meter). Second, the pressure valve of the installation jet was set, so that the manometer at 0 meter indicated the intended pressure. Since the pressure had to develop over the length of the duct, the manometer had to be checked again after a few minutes and, if necessary, the pressure valve had to be re-adjusted to the required value. Calibrating the manometer of the jet in this way, resulted in settings of its valve that corresponded to the required pressures. Therefore, to have unbiased data, during the test, the pressure valve of the jet was ought not to be changed. Similarly, the pressure of the pneumatic motor of the jet which is the pushing force motoring the cable at the inlet, was ought not to be changed during the test as well. Once the required initial pressure had been achieved, the manometers started recording the data. At the same time, the pneumatic motor was started so as to move the cable through the duct.

3.2 Specifications

The test trajectory in Haaksbergen had a length of 500 meters and was arranged in the shape of an "eight" with a radius of 4 m. Therefore, one loop through the "eight" corresponded to a distance of:

$$2 \cdot (2\pi r) \approx 50 \text{ m}.$$

Since the distance between two consecutive measurement points was also 50 meters, the manometers were located close to each other, which was an advantage when collecting the data. The duct used in the experiments had a 14 mm outer diameter and a 10 mm inner diameter. The experiments have been performed using two different cables; the first cable installed in the duct had a diameter of 7.8 mm and the second cable had a diameter of 6.0 mm. The jet used for the installation is a pneumatic jet suitable for these types of cable and duct. Neither the cable nor the duct was lubricated during the tests, however, the jet was grounded to reduce the amount of static electricity. For the measurements itself, three digital manometers were used. The consequence of this was that every test had to be executed multiple times in order to collect the data from all the measurement points.

Since the tests were rather time consuming and only 3 of the 10 measurement points could be used at the same time, the tests were performed over several days. Therefore, the ambient conditions were different for every test. The temperature stretched from 15 °C to 35 °C, the relative humidity stretched from 16% and 73% and the overall weather conditions stretched from clouded to sunny. Since the tests were performed under all kinds of different ambient conditions, overall the ambient conditions should not bias the results.

3.2.1 Design of Experiment

To validate the model as accurate as possible, several parameters were varied throughout the experiments. First, to vary the difference between the diameter of the cable and the inner diameter of the duct, two cables with different diameters were used in the experiments, as mentioned in Subsection 3.2. Note that by varying the cable diameter not only the difference but also the ratio was varied. Second, the length of the trajectory was varied; i.e. the length of the trajectory was reduced from 500 to 300 m for some experiments. Third, the pressure at the inlet was set to either 6 or 11 bar. Varying these three parameters resulted in eight different test scenario's. However, due to the limited number of manometers all scenario's had to be executed multiple times. To eliminate the influence of noise (e.g. temperature and other ambient conditions), the order in which the experiments were executed was randomized. The length of the trajectory and the pressure at the entrance were easy to vary. However, varying the cable diameter required the machine to be manipulated which was rather time consuming. Therefore, all experiments with the 6.0 mm cable were executed first (in a random order), after which the experiments with the 7.8 mm cable were performed (again in a random order). Table 1 gives an overview of the settings of the different parameters throughout the experiments.

Table 1: The high and low settings for the parameters throughout the experiments.

parameter	low setting	high setting
cable diameter	6.0 mm	7.8 mm
trajectory length	300 m	500 m
pressure at inlet	6 bar	11 bar

3.3 Monitoring the Installed Length

The manometers output the pressure at a specific point in the duct over time. However, the models used to calculate the pressure are based on the position of the head of the cable rather than on time. Therefore, it is important to record the installed length of the cable over time such that afterwards the pressure over time can be transformed into pressure over installed length. Hence, every 10 meters of installed cable (indicated by the jet) the elapsed time was recorded using a stopwatch. This resulted in a table containing the position of the cable head and the corresponding elapsed time which was used to convert the data from the manometers. However, in most cases the cable reached the end of the trajectory be-

fore the odometer of the jet indicated so, especially when the speed of the cable was rather low (<20 m/min). This obviously causes a bias when converting the data and has to be taken into account when analyzing the results. This phenomenon is discussed further in Subsection 6.2

4. Results

This section shows two examples of the results. First the interpretation of these results will be discussed.

4.1 Interpretation of the Results

The results are shown in figures with on the y-axis the pressure in bar and on the x-axis the position of the cable head X in m. Every graph in the figure represents the data from one manometer. This means that one graph represents the pressure at one point x in the duct for different positions of the cable head X (the x-axis). So, if the model is correct, each graph corresponds to the pressure according to Equation 17, for a fixed x and a varying X. Note that this fixed x is different for every graph.

4.2 Results

Figure 4 shows the results for a 6.0 mm cable, a trajectory length of 500 m and a pressure at the inlet of 6 bar. The "dips" occur every 50 meters which is exactly the point where the cable passes the manometer. This supports the hypothesis because after the cable has passed, the air has only the annulus between the cable and duct to flow, which is far less than the duct without cable. Therefore, the pressure will initially decrease and after the cable has passed it will increase towards its initial value.

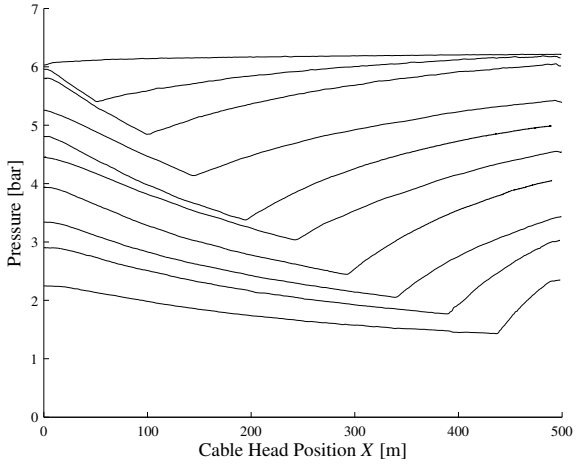

Figure 4: The pressure inside the duct measured every 50 meters of the 500 m trajectory for a moving 6.0 mm cable and a pressure at the inlet of 6 bar.

Figure 5 shows the results for a 7.8 mm cable, a trajectory length of 300 m and a pressure at the inlet of 11 bar. The "dips" are much deeper than in Figure 4, this also supports the hypothesis because in Figure 5 the diameter of the cable is larger. A larger cable diameter D_c results in a larger difference between the duct diameter D_d (emty duct) and the resulting diameter D_r (duct with a cable inside). Therefore, the pressure drop is higher for large cable diameters.
Furthermore, it can be seen that in both figures the graphs return to their initial pressure, i.e. for each graph the pressure at $X = 0$ equals the pressure at $X = L$.

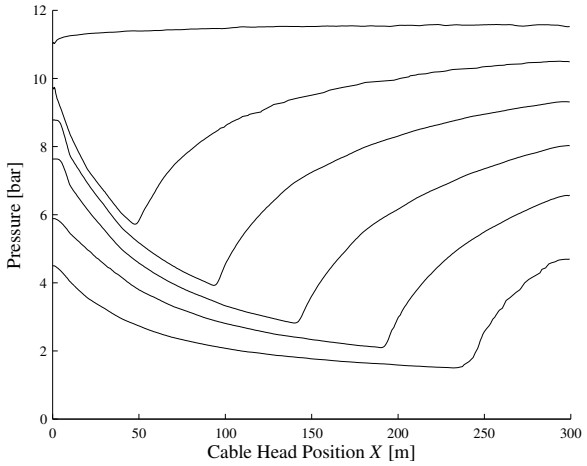

Figure 5: The pressure inside the duct measured every 50 meters of the 300 m trajectory for a moving 7.8 mm cable and a pressure at the inlet of 11 bar.

5. Analysis

In this section the results of the tests are analyzed and the optimization of the model is presented. First filtering of the data is discussed.

5.1 Filtering

Before analyzing the results, the raw data from the manometers is filtered using a running average filter:

$$Y_i = \frac{1}{5}\left(y_{i-2} + y_{i-2} + y_i + y_{i+1} + y_{i+2}\right)$$

with y_k being the raw data and Y_k the filtered data. This results in a smoother signal, than the raw data from the manometers. Filtering is necessary because the raw data is rather noisy, although this is only visible when zooming in on the data and not in, for example, Figure 4.

5.2 Error Calculation

In the analysis of the results, the pressure as measured by the manometer of the installation jet is taken as the actual pressure at the inlet instead of the target pressure (6 or 11 bar, depending on the test). Although the pressure of the installation jet is not changed manually, it changes of its own accord as the tests proceed, as can be seen in Figures 4 and 5; the graph in the top of the figure slightly increases where it should be constant. So, this phenomenon will be taken into account when analyzing the results.
To analyze the results, the "dips" in the measurements are compared to the "dips" predicted by the model (17). For one setting of the variables (see Table 1) the absolute difference between the model prediction and either the five or nine measurements, depending on the length of the trajectory, is calculated. Formally, this can be written as

$$E_{500,p_1,D_c} := \sum_{k=1}^{9} |m_k(50\cdot k) - p(50\cdot k, 50\cdot k)| \qquad (18)$$

$$E_{300,p_1,D_c} := \sum_{k=1}^{5} |m_k(50\cdot k) - p(50\cdot k, 50\cdot k)| \qquad (19)$$

with $m_k(a)$ being the measurement of the manometer at $(50 \cdot k)$ meters from the start of the trajectory when a meters of cable was installed. Furthermore the subscripts p_1 and D_c indicate the pressure at the inlet and the cable diameter corresponding to the setting of the parameters of the test. For the sake of simplicity these subscripts are omitted for $m_k(a)$ and $p(x,X)$.
Note that the error for $k = 0$ is not incorporated in this equation. This is because the measurement of the manometer directly after the jet, corresponding to $k = 0$, is taken as the pressure at the inlet instead of the target pressure. So this would result in an imposed error of zero at $k = 0$ which obviously affects the results unfairly.
To calculate the error of the model for all collected data, the error for each of the eight settings of the parameters (see Table 1) is calculated and averaged:

$$E := \frac{1}{56}\left(E_{500,6,6.0} + E_{500,6,7.8} + E_{500,11,6.0} + E_{500,11,7.8} + E_{300,6,6.0} + E_{300,6,7.8} + E_{300,11,6.0} + E_{300,11,7.8}\right). \quad (20)$$

The denominator 56 is the total number of graphs; four measurements for the 500 m trajectory with each nine graphs and four measurements for the 300 m trajectory with each five graphs $(4 \cdot 5 + 4 \cdot 9 = 56)$.

5.3 Optimization of the Model

The results can now be assessed using a norm (Equations 18 and 19) and therefore it is also possible to optimize the model regarding the resulting diameter D_r. Recall that initially this variable was chosen to be

$$D_r = \sqrt{D_d^2 - D_c^2}.$$

However, strictly speaking the resulting diameter should be the hydraulic diameter D_h, defined as four times the cross sectional area A divided by the wetted perimeter of the cross section O:

$$\begin{aligned} D_h &:= \frac{4A}{O} \\ &= D_d - D_c. \end{aligned}$$

Recently Griffioen already argued that the annulus between the cable and the duct should be considered more like an ellipse, instead of a circle [1]. Therefore a new resulting diameter D_R will be defined as a linear combination of the two equations above:

$$\begin{aligned} D_R(\lambda) &:= \lambda\sqrt{D_d^2 - D_c^2} + (1-\lambda)\cdot(D_d - D_c) \\ &= \lambda D_r + (1-\lambda) D_h \end{aligned} \quad (21)$$

with $\lambda \in [0,1]$. The error of the model will be minimized for lambda using only the data collected with the 7.8 mm cable. Then this optimal lambda will be applied to the data collected with the 6.0 mm cable to check for consistency.

5.3.1 Optimizing for Big Cable Diameter

The resulting diameter D_r in Equation 16 is replaced by the new resulting diameter $D_R(\lambda)$, as defined in Equation 21. Next the optimal lambda λ^* is defined such that the error, based on Equations 18 and 19, is minimal for the data collected with the 7.8 mm cable, i.e. minimize:

$$E_{7.8} := \frac{1}{28}\left(E_{500,6,7.8} + E_{500,11,7.8} + E_{300,6,7.8} + E_{300,11,7.8}\right).$$

Applying a numerical iteration algorithm results in the optimal value

$$\lambda^* := 0.878 \quad (22)$$

with a corresponding error

$$E_{7.8} = 0.175.$$

This means that when λ^* is applied, the model (17) is on average 0.175 bar off of the measurements with the 7.8 mm cable.

5.3.2 Comparison with Small Cable Diameter

Similar to the error for the 7.8 mm cable diameter, an error for the 6.0 mm cable data is defined.

$$E_{6.0} := \frac{1}{28}\left(E_{500,6,6.0} + E_{500,11,6.0} + E_{300,6,6.0} + E_{300,11,6.0}\right)$$

Applying the optimal lambda λ^* to the 6.0 mm cable data results in an error

$$E_{6.0} = 0.185.$$

When the model is optimized with respect to lambda for the 6.0 mm cable data, similar to the 7.8 mm cable data, the optimal value is $\lambda^\dagger := 0.882$ with a corresponding error $E_{6.0} = 0.185$. So the difference between λ^* and $\lambda^\dagger$ is very small and the difference in the corresponding errors is not significant. Therefore it can be conclude that the optimal lambda for the model is λ^*, as defined in Equation 22.

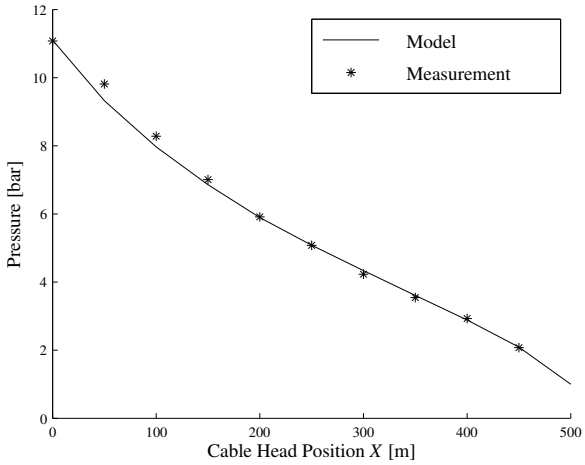

Figure 6: The "dips" of the measurements compared to the "dips" according to the model for the 6.0 mm cable, a pressure of 11 bar at the inlet and a 500 m trajectory. The stars represent the "dips" of the measurements.

5.4 Assessment of the Model

Next, the optimal lambda is applied to all data to asses the model as a whole. This will show how well the model predicts the pressure. Using the optimal lambda λ^* results in a total error of the model

$$E = 0.180$$

where E is as defined in Equation 20. This means that the model is on average 0.18 bar off of the actual pressure. Furthermore, the sample standard deviation s, defined as

$$s := \sqrt{\frac{1}{56-1}\sum_{i=1}^{5} 6(y_i - 0.180)}$$

with y_i being the individual errors, is 0.162. This means that the errors are close to the mean, i.e. the spread is small.
Figure 6 shows the "dips" of the measurements compared to the "dips" according to the model for the 6.0 mm cable, a pressure of 11 bar at the inlet and a 500 m trajectory. The error as defined in Equation 18 can be seen as the distance from a star to the line, summed over all stars.
Figure 7 shows the measurements and the pressure according to the model for the 7.8 mm cable, a pressure of 11 bar at the inlet and a 300 m trajectory. The measurements are represented by the solid lines, whereas the model is represented by the dotted lines.
Note the difference in the location of the "dips" in Figure 7, this is probably due to slipping of the cable and/or a bias in the odometer of the jet. This is discussed further in Subsection 6.2

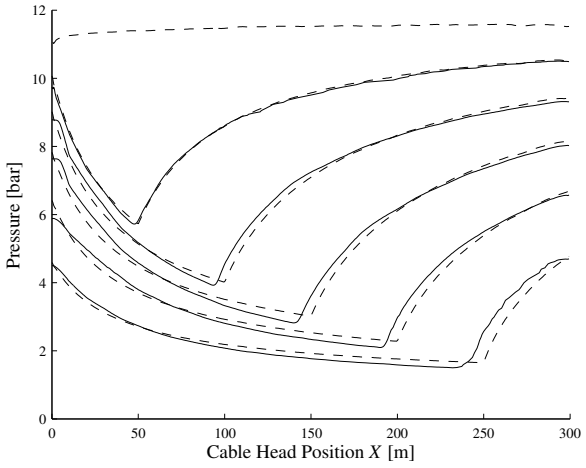

Figure 7: The pressure inside the duct every 50 m for a moving 7.8 mm cable, a pressure of 11 bar at the inlet and a 300 m trajectory. The solid lines represent the measurements and the dotted lines represent the estimation based on the model.

6. Discussion

This section will present the impact of the hypothesis on Griffioen's Model. Furthermore, some remarks regarding the test are discussed.

6.1 Impact on Griffioen's Model

According to Griffioen's model, the contribution of the air on the force build-up is mainly present in, roughly, the last 25% of the trajectory because in this part, the pressure decay increases rapidly. However, the model of the pressure profile presented in this paper shows that directly after the cable head a pressure drop is present which causes a large pressure decay, even if the cable head is not in the last part of the trajectory. This means that the contribution of the air on the force build-up is present and significant throughout the entire trajectory. As a result of this, the force build-up in the cable is significantly lower than Griffioen's model estimates. Therefore, longer installation lengths can be reached than Griffioen's model calculates. The latter has also been experienced in practice; the test performed with the 7.8 mm cable for a 500 m trajectory and a pressure of 6 bar at the entrance would not have been possible according to Griffioen's model.

Furthermore, due to the continuous presence of the significant pressure decay, the required pushing force at the entrance increases monotonically. Whereas Griffioen's model implies that the required pushing force decreases when the cable is in, roughly, the last 25% of the trajectory. This is shown in Figure 8 where, for the sake of simplicity a straight duct (with windings) is simulated. For a maximum pushing force of 115 N, Griffioen's model predicts that the cable is able to pass through a trajectory of 730 m. However the new model predicts that the cable will be able to pass through a trajectory of 840 m. Note that in both cases the same maximum pushing force is reached only at different moments during the installation, i.e. at 590 m (19% of the trajectory's end) and 840 m respectively. This phenomenon has also been experienced in practice; in all tests the speed of the cable either was constant or it decreased as the cable was pushed further into the duct. Never it was experienced that the speed increased which would be the case if the required pushing force was to decrease.

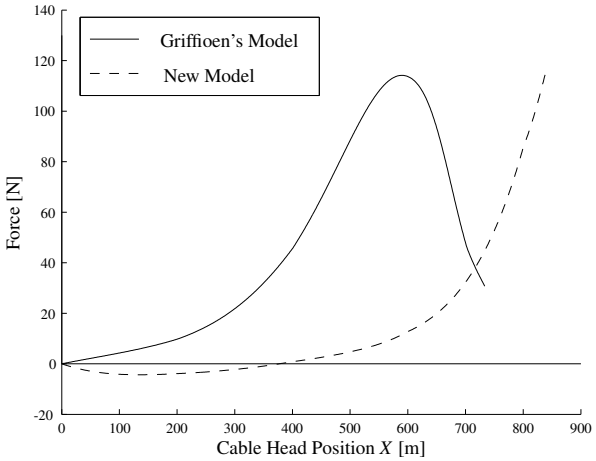

Figure 8: The required pushing force at the inlet according to Griffioen's model (solid) and according to the new model (dotted). Simulation for a 7.0 mm cable in a 10 mm duct, a pressure at the inlet of 10 bar and maximum pushing force of 115 N.

6.2 Bias in the Odometer of the Jet

Subsection 5.4 already mentioned the difference between the location of the "dips" according to the model and the measurements in Figure 7. This is probably due to slipping of the cable and/or a bias in the odometer of the installation jet. The length stamps on both the cable and the duct indicated that the length of the trajectory was either 300 m or 500 m. However, in most tests, the cable reached the end of the trajectory before the jet indicated that 300 m or respectively 500 m was installed. This difference was sometimes up to 20 meters for the 500 m trajectory. Obviously, this affects the results; a measurement for 230 m installed cable could easily belong to 250 m installed cable. Note that the discrepancies between the "dips"in Figure 7 increase as the cable is pushed further into the duct. This suggests that the bias is linear with the installed length of cable, which supports the idea that the bias is due to slipping of the cable and/or a bias in the odometer of the jet.
To avoid the influence of this probable bias, the analyses in Section 5 were performed as if the "dips" were exactly every 50 meters.

6.3 Wear of the Cables and Duct

All tests were preformed with the same duct and the same 7.8 mm and 6.0 mm cables. In total, almost 40 tests - including re-tests due to failures - were performed; this obviously causes wear to the cables and the duct. Wear of the materials affects the jetting performance of the cable and can cause a bias in the measurements. To have, from this perspective, unbiased measurements, every test had to be performed with a new duct and a new cable. However, replacing the duct and manipulating it for the manometers is a rather time consuming process. Therefore, the same materials were used in every test. Hence, the measurements may have been affected by effects due to wear of the cables and the duct.

7. Conclusion

Several tests have been performed to support the hypothesis that the pressure profile in a duct changes as the optical cable moves through the duct. Based on the results and the analysis of these results, it can be concluded that the model presented in this paper is a good estimation of the pressure in a duct with a moving cable inside. With an average error of 0.180 bar and a error spread of 0.162 bar the model estimates the actual pressure rather well. With this relatively small error, the estimation is good enough to predict installation lengths in the application of cable jetting more accurate. This new pressure profile changes the concept of the whole jetting process; instead of that the contribution of the air on the force build-up is mainly present in, roughly, the last 25% of the trajectory length (because the pressure decay would be the largest in this part), the contribution is present and significant in the entire trajectory due the pressure drop directly after the cable head. This means that the synergy of pushing and blowing at the same time is even more effective than thought. Furthermore, based on this new model, longer installation lengths can be reached which has been experienced in practice.

8. Acknowledgments

We would like to express our gratitude towards Jos Vaarwerk from BV Twentsche Kabelfabriek Haaksbergen, The Netherlands, for his commitment to the tests and for helping us with his extensive experience and practical knowledge of cable jetting.

References

[1] W. Griffioen et al. “Floating Cable into Duct: Recent Developments”. *Proceedings of the 62nd IWCS*, November 2013.

[2] W. Griffioen. *Installation of Optical Cables in Ducts*. Plumettaz SA, 1993.

[3] W. Griffioen, G. Plumettaz, and H.G. Nobach. “Theory, Software, Testing and Practice of Cable in Duct Installation”. *Proceedings of the 55nd IWCS/Focus*, November 2006.

Authors

Almar Snippe started his bachelor in Applied Mathematics at the University of Twente, The Netherlands, in 2006. After enhancing the Crankshaft Torque Monitoring System at R&D Ford Aachen, Germany (2010), for his internship, he focused on Optimal Signal Reconstruction at the University of Twente for his master thesis. In 2011 he received his M.Sc. degree in Applied Mathematics at the University of Twente. Currently he is a Ph.D. student at the University of Twente concerning the installation of optical fibers in ducts. This project is financed by BV Twentsche Kabelfabriek (TKF) in Haakbsergen, The Netherlands.

Onno Bresser received his M.Sc. degree in Electrical Engineering at the University of Technology of Delft (The Netherlands) in 1975. After that he joined NKF Kabel (later Draka) where he founded a group for development of optical fiber cable and associated technologies. From 1990 till 1995 Onno worked as an independent consultant, in which period, amongst other things, he developed optical tow cable systems for sonar systems for military surface vessels as well as submarines. In 1995 he joined TKH Group where he did build a plant for manufacturing optical fiber and cable in Nanjing (People’s Republic of China). Presently Onno is Director Development of Optical Fibre and Cable at TKH Group as well as Chief Technical Officer at Twentsche (Nanjing) Fibre Optics.

Sipke Hoekstra obtained his M.Sc. and Ph.D. degrees at the University of Twente, The Netherlands. He is currently employed as an Assistant Professor at the University of Twente, faculty of Engineering Technology, department of Design, Production and Management, section Production Management. In the nineties he developed production machines and production lines in the machine industry as a senior systems engineer and manager engineering. His current interests include manufacturing systems design and production planning and control. He is involved currently involved in the research and development project with TKF that focuses on the installation of optical fibers.

Willem Griffioen received his M.Sc. degree in Physics and Mathematics at Leiden University (NL) in 1980 and worked there until 1984. Then he was employed at KPN Research, Leidschendam (NL), working in the field of Outside-Plant and Installation Techniques. He received his Ph.D. (Optical Fiber Reliability) in 1995 at Eindhoven Technical University (NL). From 1998 to 2009 he worked at Draka Comteq, Gouda (NL), on Connectivity of FttH. Currently he works at Plumettaz SA, Route de la Gribannaz 12, CH-1880 Bex (CH), willem.griffioen@plumettaz.com and is responsible for R&D of cable installation techniques.